

# ERG Responses in Mice with Deletion of the Synaptic Ribbon Component RIBEYE

Richard Fairless,<sup>1,2</sup> Sarah K. Williams,<sup>1,2</sup> Rashmi Katiyar,<sup>3</sup> Stephan Maxeiner,<sup>3</sup> Frank Schmitz,<sup>3</sup> and Ricarda Diem<sup>1,2</sup>

<sup>1</sup>Department of Neurology, University Clinic Heidelberg, Heidelberg, Germany

<sup>2</sup>CCU Neurooncology, German Cancer Consortium (DKTK), German Cancer Research Centre (DKFZ), Heidelberg, Germany

<sup>3</sup>Institute of Anatomy and Cell Biology, Department of Neuroanatomy, Saarland University School of Medicine, Homburg, Germany

Correspondence: Richard Fairless, Department of Neurology, University Clinic Heidelberg, Im Neuenheimer Feld 350, 69120 Heidelberg, Germany; [r.fairless@dkfz-heidelberg.de](mailto:r.fairless@dkfz-heidelberg.de).

Received: September 30, 2019

Accepted: April 12, 2020

Published: May 21, 2020

Citation: Fairless R, Williams SK, Katiyar R, Maxeiner S, Schmitz F, Diem R. ERG responses in mice with deletion of the synaptic ribbon component RIBEYE. *Invest Ophthalmol Vis Sci.* 2020;61(5):37. <https://doi.org/10.1167/iovs.61.5.37>

**PURPOSE.** To determine the influence of RIBEYE deletion and the resulting absence of synaptic ribbons on retinal light signaling by electroretinography.

**METHODS.** Full-field flash electroretinograms (ERGs) were recorded in RIBEYE knock-out (KO) and wild-type (WT) littermate mice under photopic and scotopic conditions, with oscillatory potentials (OPs) extracted by digital filtering. Flicker ERGs and ERGs following intravitreal injection of pharmacological agents were also obtained under scotopic conditions.

**RESULTS.** The a-wave amplitudes were unchanged between RIBEYE KO and WT mice; however, the b-wave amplitudes were reduced in KOs under scotopic, but not photopic, conditions. Increasing stimulation frequency led to a greater reduction in RIBEYE KO b-wave amplitudes compared with WTs. Furthermore, we observed prominent, supernormal OPs in RIBEYE KO mice in comparison with WT mice. Following intravitreal injections with L-2 amino-4-phosphonobutyric acid and *cis*-2,3 piperidine dicarboxylic acid to block ON and OFF responses at photoreceptor synapses, OPs were completely abolished in both mice types, indicating a synaptic origin of the prominent OPs in the KOs. Conversely, tetrodotoxin treatment to block voltage-gated Na<sup>+</sup> channels/spiking neurons did not differentially affect OPs in WT and KO mice.

**CONCLUSIONS.** The decreased scotopic b-wave and decreased responses to increased stimulation frequencies are consistent with signaling malfunctions at photoreceptor and inner retinal ribbon synapses. Because phototransduction in the photoreceptor outer segments is unaffected in the KOs, their supernormal OPs presumably result from a dysfunction in retinal synapses. The relatively mild ERG phenotype in KO mice, particularly in the photopic range, is probably caused by compensatory mechanisms in retinal signaling pathways.

Keywords: RIBEYE, synaptic ribbons, electroretinogram, oscillatory potentials

Ribbon synapses, present within sensory neurons that utilize graded synaptic signaling, are continuously active synapses that support high rates of sustained exocytosis for prolonged periods of time.<sup>1,2</sup> This is achieved through a specialization of the active zone that contains a large proteinaceous structure, the “ribbon.” The ribbon is associated with a large pool of synaptic vesicles ready for release. It has been proposed to act as a conveyor belt to provide continuous delivery of vesicles for tonic release or, alternatively, to control replenishment of readily releasable pools in order to achieve a “timing belt.”<sup>3–5</sup> These continuously active synapses are capable of slow, continuous, and fast stimulus-synchronous synaptic vesicle exocytosis.<sup>2</sup>

Within the retina, ribbon synapses are present in the outer plexiform layer (OPL), where rod and cone photoreceptors transmit light-evoked signals to bipolar cells at the first synapse of the visual system, as well as in bipolar cell-retinal ganglion cell/amacrine synapses in the inner plex-

iform layer (IPL) of the retina. In the OPL, light signals transmitted by the photoreceptor synapse are funneled into ON and OFF pathways that are equipped with different sets of metabotropic and ionotropic glutamate receptors.<sup>6,7</sup> Rod synapses nearly exclusively feed ON signaling pathways at invaginating ribbon synapses; cone synapses feed both ON and OFF pathways via multiple types of cone bipolar cells.<sup>8–10</sup> In the synapses of the inner retina in the IPL, these signals are computed via ionotropic glutamate receptors and lateral interactions with amacrine cells before being transmitted to the visual brain centers by the retinal ganglion cell axons that form the optic nerve.<sup>7–11</sup>

RIBEYE is a unique and essential structural component of the synaptic ribbon.<sup>12,13</sup> Its indispensable function was demonstrated through the deletion of RIBEYE in mice, which resulted in a complete loss of presynaptic ribbons in retinal synapses.<sup>13</sup> In addition, paired recordings in retinal slices prepared from these mice revealed that both

fast and sustained neurotransmitter releases were severely impaired in ribbon synapses between rod bipolar and AII amacrine cells. Furthermore, spontaneous miniature releases became sensitive to the slow calcium buffer EGTA, suggesting that RIBEYE may facilitate the coupling of synaptic vesicle exocytosis to calcium channels by positioning release-ready synaptic vesicles in their proximity.<sup>13</sup>

In order to determine the influence of synaptic ribbons on the electroretinogram (ERG) response to light stimulation, we performed full-field ERG recordings in RIBEYE knock-out (KO) mice in comparison with their wild-type (WT) littermates. Our results indicate no change of phototransduction in the outer segments of photoreceptors in KO mice, but disturbances of synaptic transmission occurred at ribbon synapses in the outer and inner retina.

## MATERIALS AND METHODS

### Animals

RIBEYE knock-out mice were maintained and genotyped as previously described.<sup>13</sup> Heterozygous mice were bred with each other to generate knock-out and control mice in the same litter. A total of 38 RIBEYE knock-out and 41 wild-type littermate mice (with an average age of 22.66 and 22.56 weeks, respectively) were included in the study. Mice were kept under environmentally controlled, pathogen-free conditions with free access to food and water and were maintained on a 12-hour (06:00–18:00) light/dark cycle. Animal experiments were performed during the hours of 09:00 and 13:00. All experiments involving animal use were approved by the authorities of Baden-Württemberg, Germany, and Saarland, Germany, and performed in compliance with the ARVO Statement for the Use of Animals in Ophthalmic and Vision Research.

### Electroretinography Recordings

Full-field ERGs were performed on RIBEYE knock-out and wild-type mice according to previously published procedures.<sup>14,15</sup> Mice were dark adapted overnight and anesthetized with ketamine (150 mg/kg) and xylazine (10 mg/kg), and the pupils were dilated with 0.5% atropine (Ursapharm, Saarbrücken, Germany). ERGs were recorded using the UTAS Visual Diagnostic System (LKC Technologies, Gaithersburg, MD, USA) and a contact lens electrode with gold contact (LKC Technologies). The electrical contact, as well as prevention of eye desiccation, was facilitated through application of Liquifilm OK (Allergan, Westport, Ireland). Reference and ground needle electrodes were placed subcutaneously in the neck and tail, respectively. A heating pad controlled by a rectal temperature probe was maintained at 37°C.

A single eye per mouse was recorded from and taken as an individual data point. Functional analyses included single-flash ERGs under dark-adapted (no background illumination, 0 cd·s/m<sup>2</sup>) and light-adapted (with a background illumination of 30 cd/m<sup>2</sup>, beginning 10 minutes before recording) conditions. Single white flash intensity series ranged from -4.0 to 1.5 log cd·s/m<sup>2</sup>. A total of 10 responses were averaged with interstimulus intervals of 5 (for -4.0 to -0.5 log cd·s/m<sup>2</sup>) or 17 (for 0 to 1.5 log cd·s/m<sup>2</sup>) seconds. For all ERG recordings (except scotopic threshold recordings), band-pass cutoff frequencies were 0.3 and 300 Hz.

The b-wave amplitudes were measured using raw ERG waveforms; however, to exclude oscillatory potentials (OPs) confounding the b-wave amplitude measurements, prior to measurement a smoothing algorithm was applied using EMWin software provided with the UTAS Visual Diagnostic System (LKC Technologies).

### Flicker ERG Stimulation

To determine full-field flash ERG responses with increasing frequency stimulation, dark-adapted mice were presented with 0 log cd·s/m<sup>2</sup> intensity flashes using a flicker ERG protocol at frequencies ranging from 1 to 20 Hz, again using the UTAS Visual Diagnostic System. One-second recordings were made and averaged over 20 recordings (sampling rate, 1000 Hz). Due to the potential for retinal bleaching as a result of high-frequency stimulation, after the highest frequency (20 Hz) was recorded the lowest (1-Hz) step was repeated to confirm its reproducibility, and the retina remained intact.

### Oscillatory Potential Analysis

In order to measure the OPs from flash ERG traces, the fast wavelets on the ascending edge of the b-wave were isolated using the EMWin software filtering system provided with the UTAS Visual Diagnostic System. The waveforms were digitally filtered using an algorithm that applied a smooth-and-subtract finite impulse response high-pass filter, with a frequency centered on 75 Hz. The summed OP amplitude was then measured using an automated function that identifies up to five OP wavelets within a time range beginning 3/4 of the way down the leading edge of the a-wave and ending at 55 ms after time 0 (time of light flash). Successive maxima and minima were determined by the largest and smallest current points occurring within a ±4-ms window.

### Scotopic Threshold Responses

In order to record the scotopic threshold responses (STRs), ERG signals were recorded as outlined above but with the following changes: band-pass settings were set between 0.3 and 30 Hz, flash stimulation was provided at -3.0 log cd·s/m<sup>2</sup>, and recordings were made using 30 repeats with an interstimulus interval of 5 seconds.

### Drug Application

Drugs were delivered by intravitreal injection. Eyes were punctured at the sclera junction using a 30-gauge needle, followed by insertion of a fine needle point. All drugs were dissolved in sterile PBS, and a volume of 2 µl containing 20-mM L-2 amino-4-phosphonobutyric acid (APB), 40-mM *cis*-2,3 piperidine dicarboxylic acid (PDA), and 20-µM tetrodotoxin (TTX) (all from Sigma-Aldrich, St. Louis, MO, USA) or PBS alone was injected. Recordings were performed after a 60-minute recovery time, during which time the mice were dark adapted, and they were completed within 90 minutes following injections. Eyes had not been previously injected.

### Visual Evoked Potential Recordings

Visual evoked potentials (VEPs) were measured using the UTAS Visual Diagnostic System on mice maintained at 37°C

and whose pupils had been dilated with 0.5% atropine and protected with the Liquifilm as for ERGs. Prior to recording, holes were drilled into the skull under ketamine/xylazine anesthesia (150 mg/kg and 10 mg/kg, respectively) at 3 mm lateral to lambda. Following dark adaptation for 15 minutes, needle-type electrodes were placed through the holes at a depth of ~0.5 mm into the primary visual cortex, and reference electrodes were placed subcutaneously in the neck and tail, respectively. Flash stimulation was then presented at 0 log cd·s/m<sup>2</sup> light intensity at 2 Hz with a total of 100 sweeps averaged per recording.

### Transmission Electron Microscopy of Cone Photoreceptor Synapses from Mouse Retina

Processing of mouse retina of RIBEYE knock-out mice and control mice for transmission electron microscopy (TEM) was performed largely as previously described.<sup>13</sup> The posterior eyecups with the attached retina were isolated from the eyes within 5 minutes postmortem. The dissected posterior eyecups were fixed with 4% paraformaldehyde (w/v) in PBS and subsequently with 2.5% glutaraldehyde (v/v) in PBS (12 hours each at 4°C). Samples were osmicated with 1% OsO<sub>4</sub> in 100-mM cacodylate buffer (1 hour at 4°C) and contrasted with 2% uranylacetate in 50-mM Na maleate buffer (pH 5.0) for 3 hours at 4°C. Samples were dehydrated in an ascending concentration series of ethanol and were finally equilibrated with propylene oxide (each step for 20 minutes at room temperature). Propylene oxide was gradually replaced by Epon (Shell Chemical Company, San Francisco, CA, USA)/propylene oxide mixtures, as described.<sup>13</sup> Samples were infiltrated two times with pure Epon resin (~10 hours each) before polymerization at 60°C for ~36 hours.

TEM analyses of ultrathin sections (~50–70 nm thick) were performed with a FEI Tecnai 12 BioTwin transmission electron microscope (Thermo Fisher Scientific, Waltham, MA, USA) operated at 100 kV, as previously described.<sup>13</sup> TEM images were acquired with a MegaView III digital TEM camera (Olympus Soft Imaging Solutions, Münster, Germany) controlled by Olympus iTEM acquisition software. Photoreceptor synapses are highly enriched in the OPL.<sup>16</sup> The majority of photoreceptor synapses are formed by rod photoreceptors, with cone photoreceptors representing only a minority of total photoreceptors in mice (less than 5% in mouse retina).<sup>16–18</sup> Cones could be easily discriminated from rod photoreceptors at the ultrastructural level by several criteria.<sup>9,16,19–21</sup> Cone synapses are located closer to the inner nuclear layer, and cone terminals are considerably larger than rod terminals (typically 3–5 μm in diameter in comparison to 1.5 μm of rod terminals). Rod synapses possess a single large active zone with a single large ribbon, whereas cone terminals contain multiple active zones with multiple smaller synaptic ribbons. The presynaptic active zone is opposed by a typical, characteristic assembly of postsynaptic dendrites from horizontal and bipolar cells. For the ultrastructural analyses and the subsequent quantitative evaluation, we determined whether synaptic ribbons were present in the cone pedicles. For this purpose, we analyzed whether at least one synaptic ribbon was present in a typical cone pedicle in which at least one active zone could be clearly identified by the described criteria. Ultrathin sections from five individual mice of each mouse type

obtained from four different electron microscopy embeddings were analyzed for each genotype.

### Statistical Analyses of Electron Microscopic Data

The portion of cone pedicles that contained ribbons in the two experimental groups (RIBEYE knock-out and control) was determined, as described above. Shapiro–Wilk and Kolmogorov–Smirnov tests were used to determine whether or not the data points were normally distributed. Electron microscopy data points were not normally distributed. Kruskal–Wallis statistical analyses revealed that the data points of the individual mice within the same experimental group (knock-out group, experimental group) did not differ significantly from each other. Therefore, electron microscopy results obtained from the five different mice of each group were pooled before statistical comparison with the reference group using Mann–Whitney *U* tests. Statistical analysis was performed with GraphPad Prism 8 (GraphPad Software, La Jolla, CA, USA).

### Statistics of ERG Experiments

For all ERG analyses, only one eye per animal was used and treated for statistical purposes as a single value. All data are presented as their mean values ± SEM. Statistical analysis was performed with GraphPad Prism 8. Data were assessed for normality using the Shapiro–Wilk test with subsequent assessment for statistical significance using the two-tailed Student's *t*-test (for normally distributed data) or the Mann–Whitney rank-sum test (for non-normally distributed data). Statistical significance for multiple datasets was determined using the Bonferroni–Dunn method. *P* ≤ 0.05 was considered statistically significant.

## RESULTS

### RIBEYE Knock-Out Mice Have Reduced Scotopic b-Wave Amplitudes

We first determined the flash ERG response of RIBEYE knock-out mice and their corresponding wild-type littermates in order to assess the global retinal response. This was achieved by either light adapting (for photopic measurements) or dark adapting (for scotopic measurements) the mice prior to flash ERG stimulation. The a-waves (initial negative component of the ERG waveform, generated by the photoreceptors) and the b-waves (subsequent positive component, derived mainly from ON bipolar cell activity) were then measured. The photopic ERG responses were unchanged between RIBEYE knock-out and wild-type mice, in either the a- or b-waves (Figs. 1C, 1D). In contrast, the dark-adapted response of RIBEYE knock-out mice had reduced b-wave amplitudes compared with wild-types, which were apparent in the stimulation range of –1.5 log cd·s/m<sup>2</sup> or above where amplitudes exceeded 100 μV (*P* < 0.01) (Fig. 1D). The lack of difference between the wild-type and knock-out mice under photopic conditions may reflect the smaller amplitudes of responses elicited following light adaptation and the differential contributions of rod and cone photoreceptor synaptic signaling that also include OFF responses.

Although it has previously been shown that ribbon synapses are absent from retinal synapses, including photoreceptors,<sup>13</sup> the differences observed between the

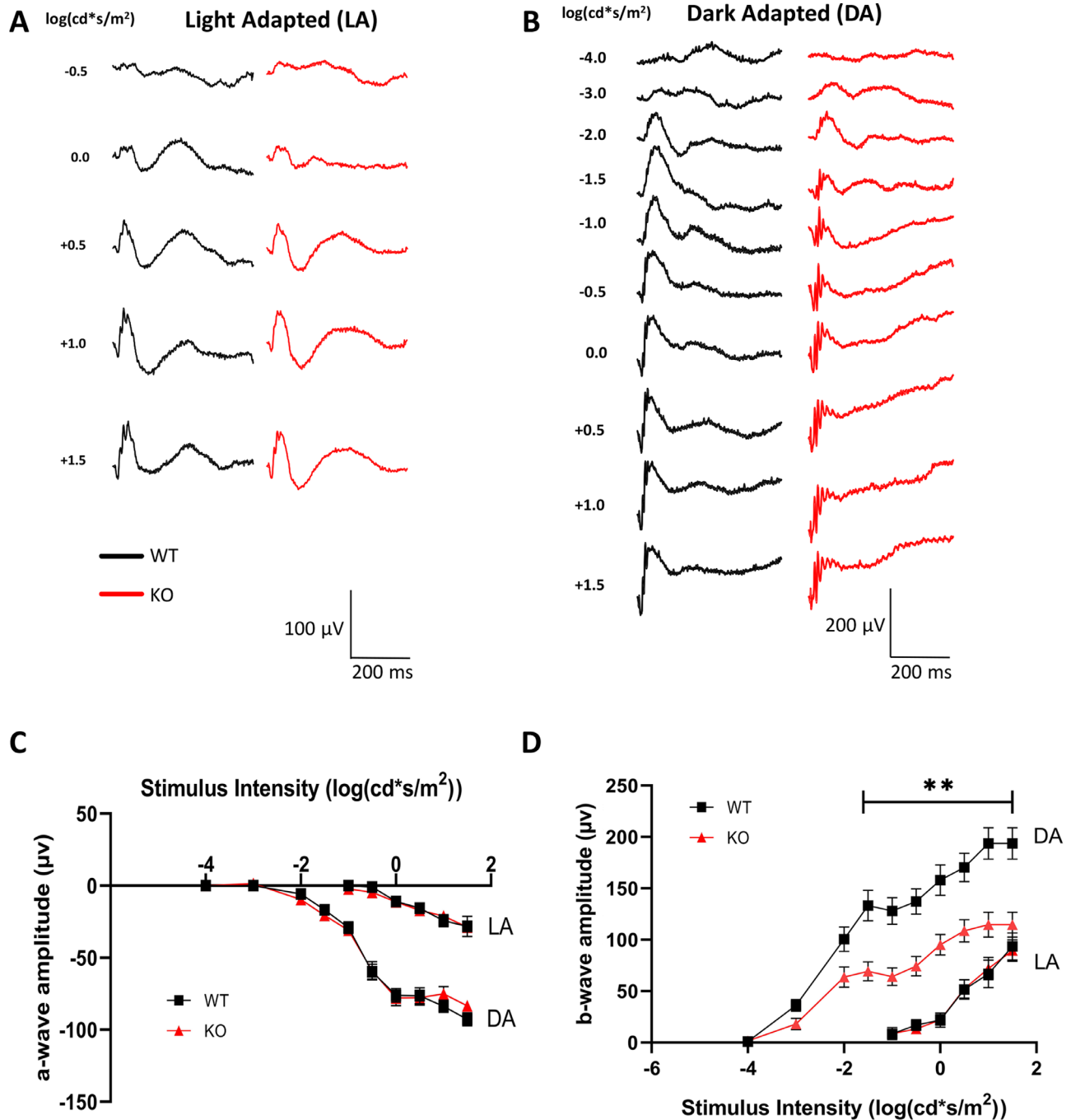


**FIGURE 1.** RIBEYE knock-out mice have reduced scotopic, but not photopic, electroretinographic responses. **(A)** Representative light-adapted (LA, photopic) and **(B)** dark-adapted (DA, scotopic) single-flash intensity series of RIBEYE wild-type (WT, *black*) and knock-out (KO, *red*) mice. Quantification of the **(C)** a-wave and **(D)** b-wave amplitudes is shown. For photopic ERG measurements,  $n = 7$  wild-type and  $n = 8$  knock-out mice (single eye per mouse); for scotopic ERG recordings,  $n = 14$  wild-type and  $n = 16$  knock-out mice (single eye per mouse).  $^{**}P < 0.01$  (Student's *t*-test with Bonferroni-Dunn correction).

photopic and scotopic ERG responses reported here may reflect a persistence of synaptic ribbons in the cone photoreceptors. To determine if this was the case, ultrastructural analyses of cone synapses were performed. Cone terminals were identified according to the criteria given above. Ultrastructural analyses by electron microscopy confirmed the lack of synaptic ribbons within cone photoreceptor synaptic terminals (Fig. 2). Previously, it has been shown that synaptic ribbons are absent from rod photoreceptor synaptic termi-

nals in RIBEYE knock-out mice,<sup>13</sup> which was confirmed in this study (Fig. 2B3).

Because ablation of RIBEYE protein results in a loss of presynaptic ribbons in retinal synapses<sup>13</sup> with subsequent reduction in the readily releasable synaptic vesicle pool, we wished to determine the ERG response following high-frequency stimulation. This was achieved through the use of a flicker ERG protocol that presented flash stimulation with an increasing frequency from 1 to 20 Hz. The

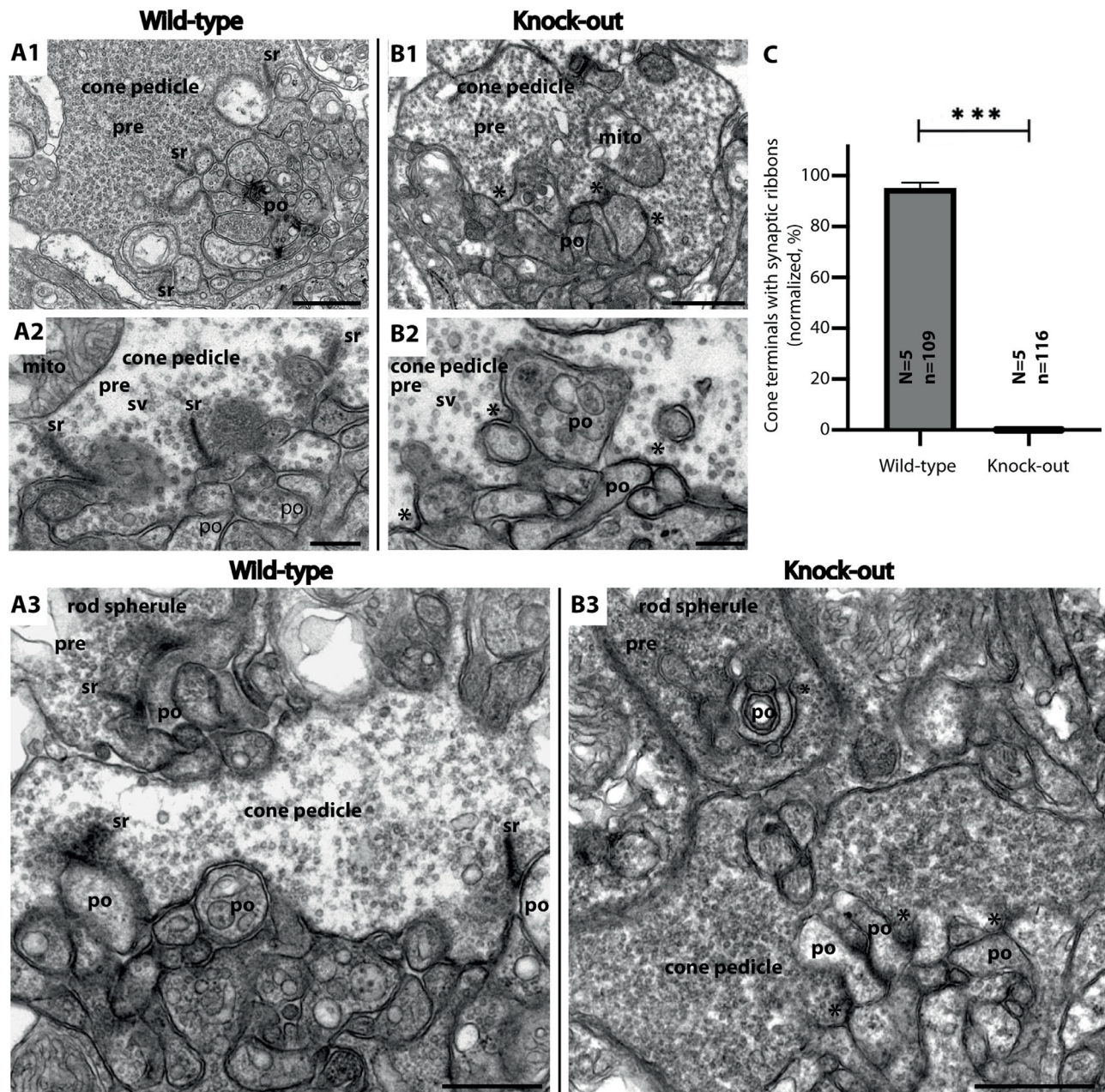


**FIGURE 2.** RIBEYE knock-out mice lack synaptic ribbons at cone photoreceptor synapses. Electron microscopic images of cone photoreceptor synapses in (A1) wild-type and (B1) knock-out mice. Higher magnification images of cone synapses are given for (A2) wild-type mice and (B2) knock-out mice. Synaptic ribbons in the wild-types are indicated by “sr,” whereas asterisks indicate the absence of synaptic ribbons at the indicated positions in RIBEYE knock-out presynaptic terminals. Electron microscopic images containing examples of both rod and cone presynaptic synapses are given in (A3) wild-type and (B3) knock-out mice. (C) Quantification of cone synaptic terminals containing synaptic ribbons and sample numbers are indicated on the bar graph (N, number of mice; n, number of synapses). \*\*\* $P < 0.0001$  (Mann-Whitney  $U$  test). Scale bars: 1  $\mu\text{m}$  (A1, B1), 500 nm (A2), 400 nm (B2), and 1  $\mu\text{m}$  (A3, B3). mito, mitochondria; pre, presynaptic terminal; sv, synaptic vesicle; po, postsynaptic terminal.

elicited amplitude of the ERG responses rapidly decreased in both mouse types with increasing frequency of stimulation (Fig. 3), but were not significantly different from each other. Because the b-wave amplitudes were already reduced in the knock-out mice compared to wild-types under slow stimulation protocols (e.g., 17-second intervals were used for 0 log cd·s/m<sup>2</sup> light stimulation in Fig. 1), the amplitudes were re-analyzed relative to the amplitude elicited at the low-frequency stimulation of 1 Hz (Fig. 3C). This allowed us

to compare the drop-off rate between the two mouse types, and a significant reduction in the ERG b-wave amplitudes of the RIBEYE knock-outs compared to their wild-type counterparts could now be detected ( $P = 0.013$  for 5 Hz and  $P = 0.008$  for 10 Hz, Student's  $t$ -test with Bonferroni-Dunn correction). This suggests that RIBEYE knock-outs respond less well to high-frequency stimulations than their wild-type counterparts. This decreased global retinal response might reflect a greater depletion in the readily releasable vesicular

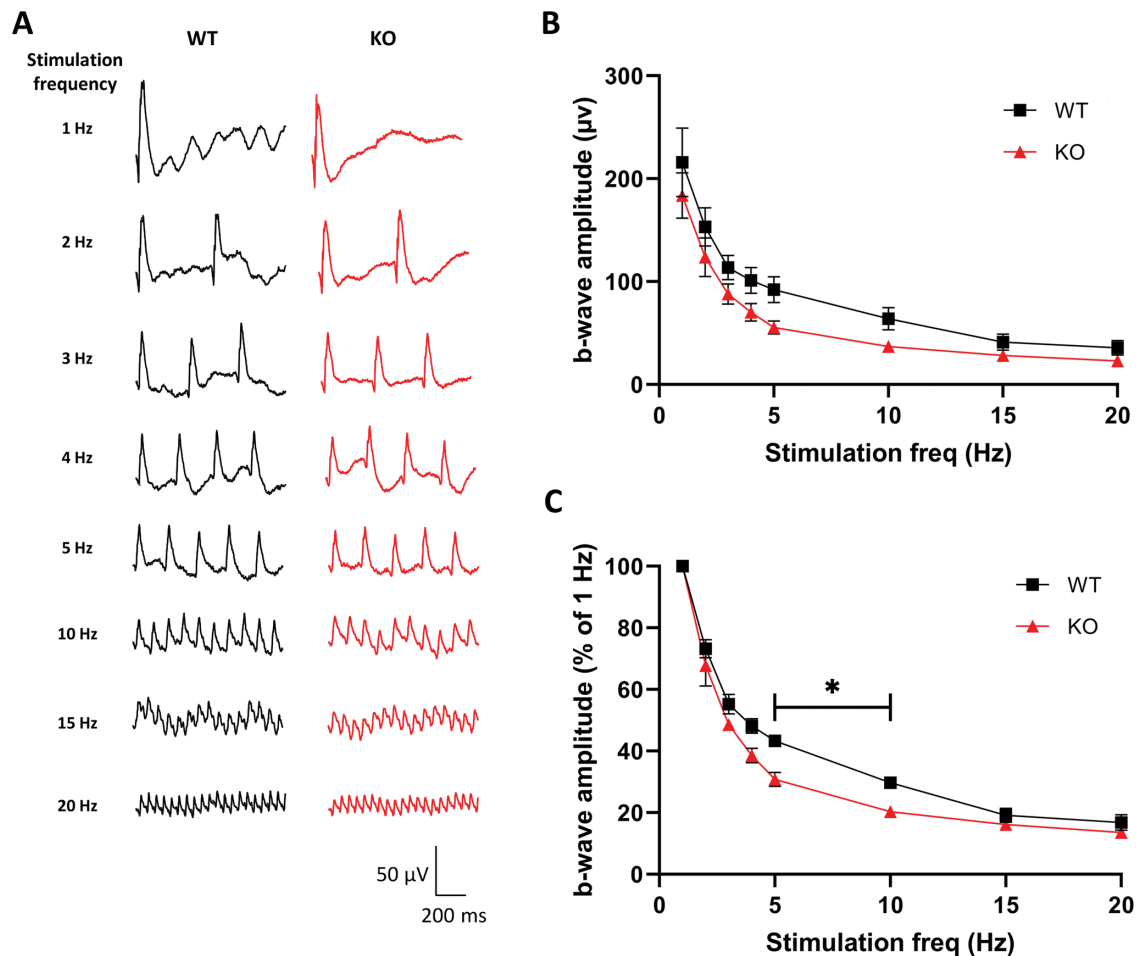


**FIGURE 3.** RIBEYE knock-out mice have reduced flash ERG response amplitudes under high-frequency stimulation. (A) Representative flicker ERG responses under dark-adapted conditions, with increasing flash stimulation frequency (stimulus intensity 0 log cd·s/m<sup>2</sup>). (B) Quantification of flicker ERG b-wave amplitudes with increasing frequency stimulation. (C) To measure the drop-off in ERG amplitude with increasing stimulation frequency, the same dataset is plotted as percent of ERG b-waves elicited at 1-Hz stimulation; n = 6 wild-type and n = 10 knock-out mice (single eye per mouse). \**P* < 0.05 (Student's *t*-test with Bonferroni–Dunn correction).

pool in RIBEYE knock-out presynapses compared with wild-types. At higher frequency stimulation rates, both wild-type and knock-out mice had vastly reduced ERG amplitude responses with no significant differences between them. At these rates, the vesicular pool might be depleted beyond replenishment capacity in both knock-outs and wild-types.

### Enlarged Oscillatory Potentials Are Apparent in RIBEYE Knock-Out Mice

One of the key differences observed between the scotopic ERG responses of RIBEYE knock-out and wild-type mice, as shown in Fig. 1B, was what appeared to be more robust OP wavelets during the ascending phase of the b-wave. In order to investigate the OPs in more detail, the OP waveform was extracted from the ERG response through the use of digital filtering, using software provided with the UTAS Visual Diagnostic System. As shown in Fig. 4A, the applied algorithm resulted in a smoothing of the a- and b-wave components, leaving the OP wavelets (OP1–OP4) remaining. Fast Fourier transform analysis (Fig. 4B) confirmed the isolation of the OP component of the ERG response.

The summed OP amplitudes were then calculated (as indicated in Fig. 4A) and compared between wild-type and RIBEYE knock-out mice (Fig. 4D). No significant differences were seen between the two mouse types, presumably reflecting the large data spread (wild-type summed OP amplitude, 238.3 ± 22.9 µV; RIBEYE knock-out, 245.1 ± 25.1 µV; *P* = 0.9, Student's *t*-test). However, it was observed that irrespective of whether a large or small ERG response was elicited, the OPs consistently dominated the shape of the RIBEYE knock-out ERG waveform (Fig. 4C). This was further seen upon averaging multiple ERG responses and superimposing them (Fig. 4F). In wild-type mice, due to slight variations in the timing of the OP wavelets, averaging of multiple ERG waveforms resulted in a smoothing of the OP wavelets. In contrast, the knock-out ERG average retained distinctive oscillations in the ascending b-wave.

In order to further investigate the contribution of OPs to the ERG waveform, the OP amplitudes were plotted with respect to the size of the b-wave as measured prior to OP extraction (Fig. 4E). A greater difference was now apparent between wild-types and RIBEYE knock-outs (average OP amplitude/b-wave of wild-types, 1.47 ± 0.09; RIBEYE knock-outs, 2.54 ± 0.14; *P* < 0.0001, Mann–Whitney *U* test), again

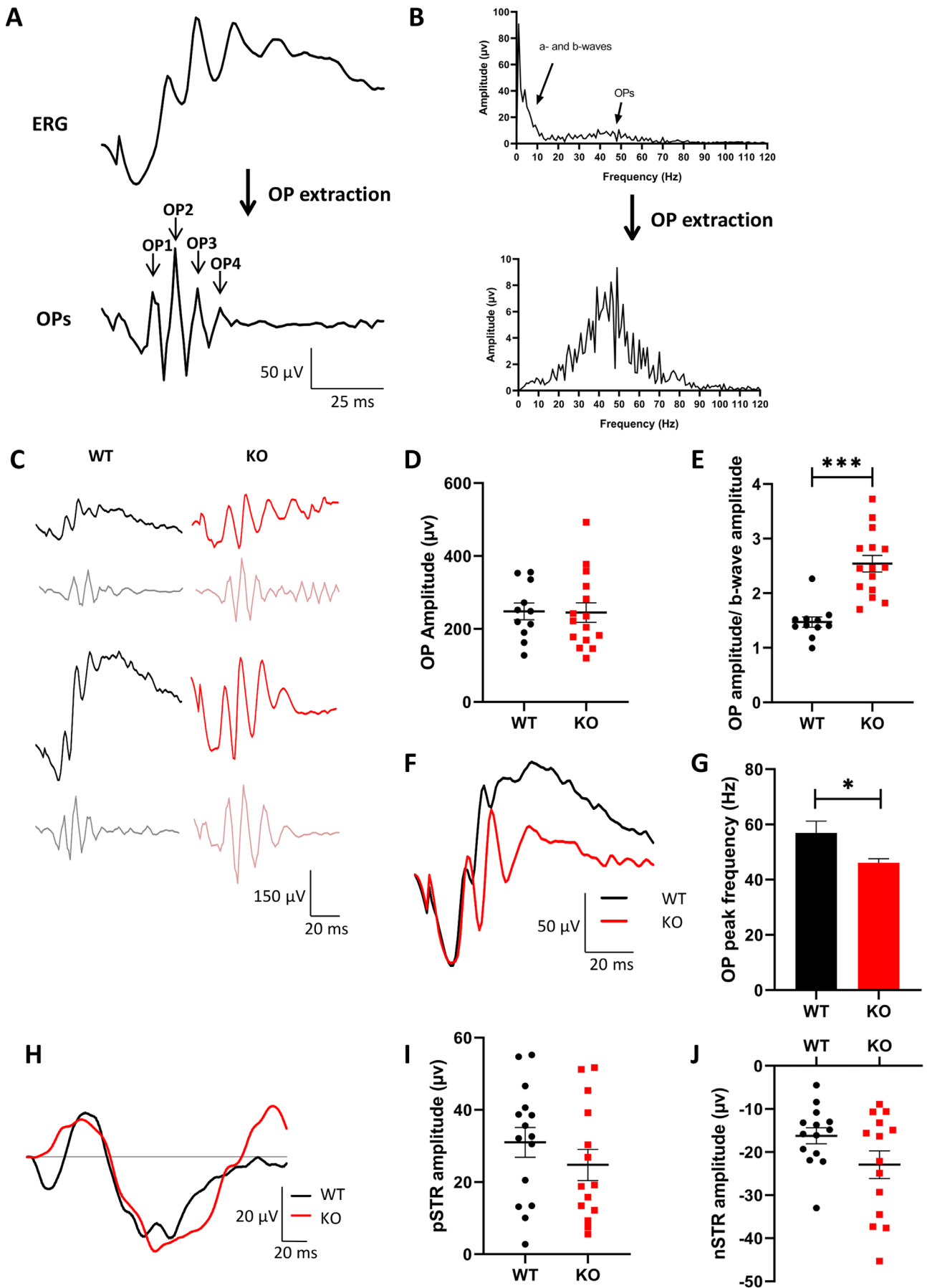


**FIGURE 4.** RIBEYE knock-out mice have more prominent OPs than wild-type mice. (A) Example of OP extraction protocol. (B) Frequency domain representation of the ERG waveform by fast Fourier transform (from the waves shown in A), demonstrating successful isolation

of the OPs from the low-frequency a- and b-wave components. (C) Example flash ERG responses (stimulation of 1-Hz frequency, 0 log cd-s/m<sup>2</sup> intensity) for small (upper) and large (lower) ERG responses demonstrating larger oscillations for RIBEYE knock-out mice in both cases (*black*, wild-type; *red*, knock-out). Isolated OPs from the ERG responses are shown in *gray* (WT) and *pink* (KO). (D) Quantification of summed OP amplitudes. (E) Data in D presented relative to the b-wave amplitude, as measured prior to OP isolation. <sup>\*\*\*</sup> $P < 0.0001$  (Mann–Whitney  $U$  test). (F) Superimposed average of pooled flash ERG responses. (G) OP peak frequencies as measured from the frequency domain representations as given in B. <sup>\*</sup> $P < 0.05$  (Student's  $t$ -test). (H) Representative STRs with quantification of the peak (I) positive (pSTR) and (J) negative components. (D, E)  $n = 11$  wild-type and  $n = 15$  knock-out mice; (F)  $n = 10$  wild-type and  $n = 10$  knock-out mice; (I, J)  $n = 15$  wild-type and  $n = 14$  knock-out mice (all single eye per mouse).

confirming the greater contribution of the OP wavelets to the shape of the ERG waveform in RIBEYE knock-outs. Another difference between the two mouse types that was apparent in the OPs was that the power spectra (represented in Fig. 4B) differed with a slightly, but significantly, lower dominant (peak) frequency (wild-type OP peak,  $56.9 \pm 4.3$  Hz; knock-out OP peak,  $46.1 \pm 1.4$  Hz;  $P = 0.01$ , Student's  $t$ -test) (Fig. 4G).

Because oscillatory potentials are believed to arise in part from inner retinal activity, we next investigated this further by recording the scotopic threshold responses. STRs are elicited under low-light conditions and are typified by a dominant negative potential generated further upstream than the b-wave and thus are believed to reflect activity of the proximal retina, such as amacrine and retinal ganglion cells.<sup>22,23</sup> The STR for both wild-type and knock-out mice consisted of a small positive wave followed by a larger negative wave (Fig. 4H). However, quantification of the positive STR (pSTR) and negative STR (nSTR) components did not reveal any statistical differences ( $P = 0.305$  for pSTR and  $P = 0.080$  for nSTR, Student's  $t$ -test) (Figs. 4I, 4J).

### Pharmacological Deconstruction of the ERG Response

Next, we wished to investigate the ERG response further using pharmacological intervention to deconstruct the various contributions of different parts of the retina. This was achieved by intravitreal injections of PBS (as a control for the injection protocol), a combination of APB and PDA to block both ON and OFF photoreceptor postsynaptic responses,<sup>24</sup> or TTX to block spiking neurons, such as ganglion cells, and various subsets of bipolar and amacrine cells in the inner retina<sup>25–32</sup> through voltage-gated Na<sup>+</sup> channel blockade.

Following co-injection of APB and PDA, the b-wave component was abolished (as has previously been reported)<sup>24</sup> as compared to eyes receiving only PBS, leaving an extended a-wave (Fig. 5A). The isolated a-wave amplitude was quantified (Fig. 5C) and found to be unchanged between the mice groups (wild-type a-wave,  $20.6 \pm 1.9$   $\mu$ V; knock-out a-wave,  $23.0 \pm 4.5$   $\mu$ V;  $P = 0.68$ , Student's  $t$ -test), in agreement with the indistinguishable a-waves as assessed prior to APB/PDA treatment (Fig. 1). Thus, it appears that the photoreceptor light response between the two mice groups was unchanged. In addition, the OPs in both wild-type and knock-out ERGs following APB/PDA application were abolished, demonstrating that the OPs arise downstream from the photoreceptors.

Voltage-dependent Na<sup>+</sup> channels have been proposed to contribute to ERG b-wave responses by different mechanisms,<sup>33,34</sup> so we therefore asked if they also contribute to the enhanced OPs in the knock-out mice. To confirm efficient delivery of the TTX, VEPs were recorded following intravitreal injection of TTX, demonstrating that they were efficiently abolished (Fig. 5B). Following injection of

TTX, the greater OP amplitude with respect to the b-wave that was seen following PBS injections (Fig. 5E; average OP amplitude/b-wave of wild-types,  $1.23 \pm 0.13$ ; RIBEYE knock-outs,  $1.91 \pm 0.18$ ;  $P = 0.02$ , Student's  $t$ -test with Bonferroni–Dunn correction) in RIBEYE knock-outs compared to wild-types was retained (average OP amplitude/b-wave of wild-types,  $1.06 \pm 0.17$ ; RIBEYE knock-outs,  $2.13 \pm 0.27$ ;  $P = 0.01$ , Student's  $t$ -test with Bonferroni–Dunn correction). Thus, the enlarged oscillatory potentials appear to be independent of Na<sup>+</sup> channel function.

### DISCUSSION

RIBEYE has been shown to be an essential component of synaptic ribbons, which occur, in addition to those of other organs such as the inner ear and pineal gland, in ribbon synapses of the retina,<sup>12,13</sup> where they are found within the presynaptic compartments occurring between photoreceptors and bipolar cells and between bipolar cells and both retinal ganglion cells and amacrine cells. Ribbon synapses are specialized contact sites that can sustain rapid synaptic vesicle exocytosis and thus maintain tonic release capable of transducing a broad bandwidth of stimulus intensities<sup>35</sup> and thus are suited to the high demands required of vision. Ablation of RIBEYE expression resulted in retinal synapses being deficient for ribbons, with a subsequent reduction in the readily releasable vesicular pool available within the presynapse.<sup>13</sup> Our analysis of the ERG response in RIBEYE knock-out mice, in comparison to their wild-type littermates, is consistent with this view on retinal ribbon synapses and provides additional insights into synaptic ribbon function at the systems level in the retina.

The first observation is that RIBEYE knock-out mice do not have a massively impaired ERG waveform and, indeed, appeared unchanged under photopic conditions, despite the lack of synaptic ribbons, as demonstrated by both immunofluorescence and electron microscopy<sup>13,36</sup> (and confirmed in this study). This suggests that synaptic communication is not completely abolished, in contrast to ERGs derived from mouse mutants of the no-b-wave variety, which lack essential components of synaptic function<sup>37–39</sup> or result in photoreceptor degeneration.<sup>40–42</sup> This is in agreement with previous studies demonstrating that, in the absence of synaptic ribbons, functional synapses develop normally between pre- and postsynaptic components, with only modest deficits being detected in synaptic function.<sup>36</sup> In addition, in the absence of synaptic ribbons, ribbon synapses (in both the outer and inner retina) show a largely normal ultrastructure.<sup>13</sup> This is also in contrast to knock-out mice, where the ribbon synapse is disturbed through deletion of, for example, either pikachurin<sup>43,44</sup> or bassoon,<sup>45</sup> resulting in a vastly altered ERG b-wave. In both of these cases, however, the architecture of the ribbon synapse is more perturbed than just an absence of ribbons as in the RIBEYE knock-out mouse. In the pikachurin knock-out mouse, an incorrectly

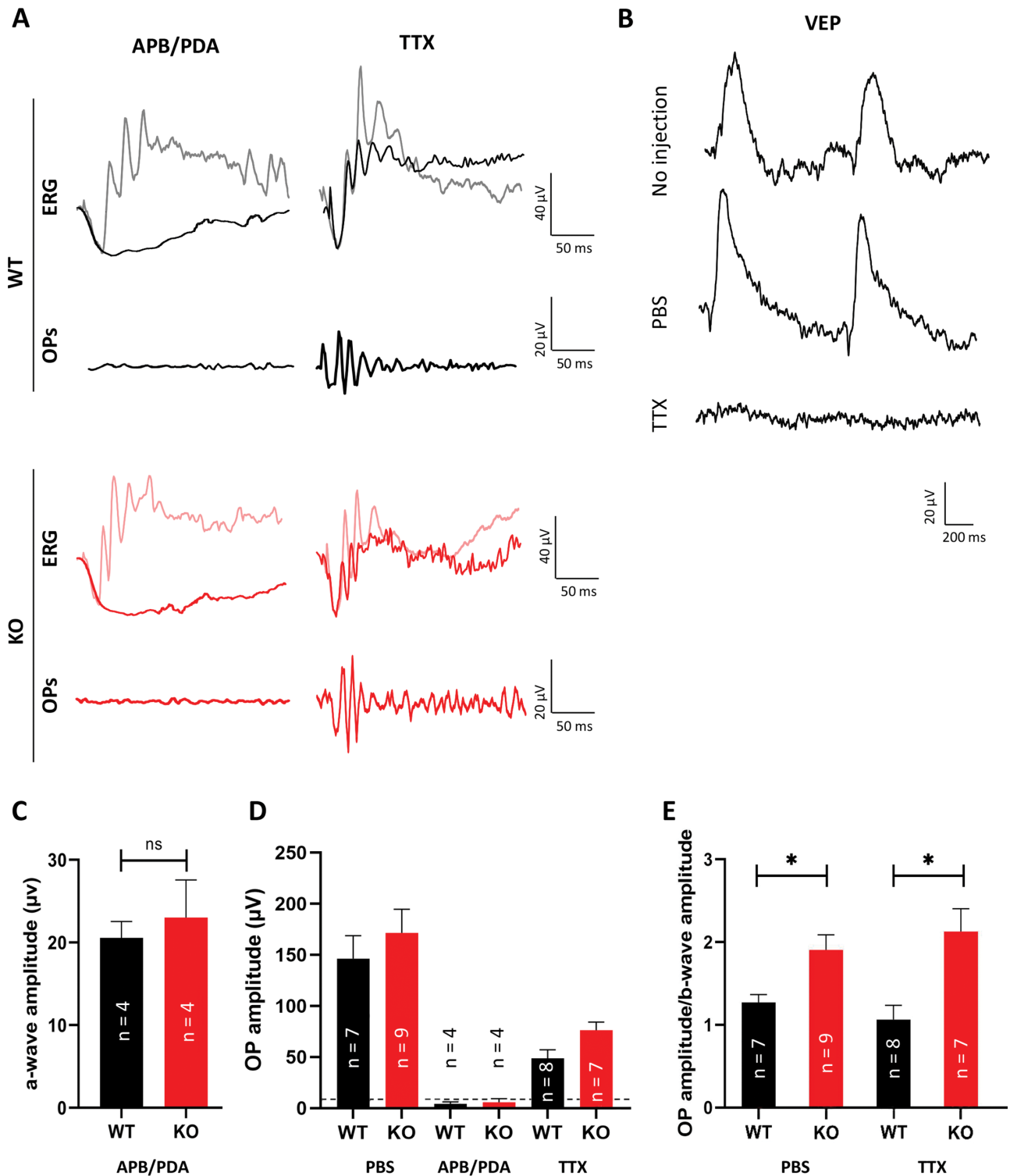


**FIGURE 5.** RIBEYE knock-out mice have unchanged a-waves but retain dominant oscillatory potentials following pharmacological isolation. **(A)** Representative flash ERG responses in wild-type (*black*) and RIBEYE knock-out (*red*) mice following intravitreal injection of either APB and PDA or TTX, as indicated (under dark-adapted conditions with 1-Hz frequency and 0 log cd-s/m<sup>2</sup> light intensity stimulation). Waveforms are superimposed onto representative PBS-injected control waveforms (WT, *gray*; KO, *pink*). OPs were extracted, and corresponding traces are given below each ERG response (WT, *gray*; KO, *pink*). **(B)** Representative VEP recordings (with 2 Hz, 0 log cd-s/m<sup>2</sup> stimulation) from wild-type mice prior to injection or following intravitreal injection with either PBS or TTX, demonstrating the inhibition of VEPs following TTX administration. **(C)** The a-wave amplitudes quantified from ERG response traces following co-injection (intravitreal) of APB and PDA. **(D)** Quantification of summed OP amplitudes following OP extraction. The noise level (OP extraction performed on traces recorded in the absence of flash stimulation) is indicated with a *dashed line*. **(E)** Data in **D** presented as OP amplitude/b-wave amplitude ratios. The numbers of eyes are provided on the bar graphs. \**P* < 0.05 (Student's *t*-test with Bonferroni–Dunn correction).

apposed ribbon synapse could be seen in relation to bipolar cell postsynaptic dendritic tips; similarly, bassoon knock-out mice had abnormal dendritic branching in the postsynaptic compartment with formation of ectopic synapses.

In contrast to photopic conditions, the amplitude of the scotopic RIBEYE KO ERG b-wave was reduced, with responses elicited with amplitudes approximately 60% of the wild-type mice. Significant differences between the mice groups were not apparent upon stimulation with low-intensity flashes (less than  $-2 \log \text{cd}\cdot\text{s}/\text{m}^2$ ) when the elicited responses were also low, indicating that synaptic vesicle fusion, in principle, can also operate in the absence of synaptic ribbons. It appears that the phenotype of the RIBEYE knock-out mice only manifests upon higher intensity stimulation, perhaps reflecting the greater demand made upon the presynaptic supply of neurotransmitter vesicles. The reduced amplitude of the scotopic b-wave is compatible with a signaling dysfunction in the outer retina, where photoreceptor synapses transmit light signals to retinal bipolar cells for further processing. The lack of difference between the mice groups under photopic conditions may reflect the smaller amplitudes of responses elicited following light adaptation and the differential contributions of rod and cone photoreceptor synaptic signaling that also include OFF responses.<sup>11,46–49</sup> The OFF responses in the outer retina originate at some distance from ribbon release sites and thus might be less dependent on the presence of the synaptic ribbon. Homeostatic mechanisms in the cone pathway, as have been observed in the inner ear (e.g., increased postsynaptic density sizes), might also contribute to the lack of defect in the photopic ERG.<sup>50,51</sup> Particularly in the cone pathway, multiple signaling and transmission pathways exist (ON, OFF, transient, sustained), represented by multiple types of cone bipolar cells that may provide the cone pathway with more options to compensate for disturbances in presynaptic release at ribbon synapses.

The rod pathway, on the other hand, predominantly feeds into a single channel via the rod bipolar cells and might be more vulnerable to a decrease in presynaptic release at the rod synapse. Moreover, it has recently become clear that cone bipolar cells also use ribbon-free contacts to a certain extent for communication, with retinal ganglion cells reducing the dependency of retinal processing on the presence of synaptic ribbons.<sup>36,41</sup> Furthermore, the difference between the ERG responses of the mice widens upon increased frequency stimulation, again reflecting an increased demand for inter-neuronal signaling. This finding is in line with the decreased frequency sensitivity of retinal ganglion cells in RIBEYE knock-outs<sup>36</sup> (which, interestingly, was also observed within the same frequency range reported here) and could be due to a disturbed coupling of the release machinery to CaV channels<sup>13</sup> that results in an altered timing of synaptic signaling.

The most apparent phenotype of the RIBEYE knock-out mice was a greater oscillatory ERG waveform. OPs are high-frequency, low-amplitude wavelets that occur on the rising edge of the b-wave. This was evident irrespective of the size of the ERG response (as demonstrated by the ratio of the OP amplitude to the b-wave responses). The molecular mechanisms underpinning OPs are not fully understood<sup>25,52–56</sup> but most likely reflect synaptic signaling at different steps of retinal processing. These include signaling at the photoreceptor synapse and predominantly synaptic processing in the inner retina, including activity of retinal ganglion cells.

That the phenotype arises at the synaptic level (or downstream of it) in the retinal circuit and not from a defect in photoreceptor sensitivity to light at the outer segment was established due to the unchanged a-waves as measured from the initial negative waveform of the ERG response and, upon isolation of the photoreceptor response, through pharmacological inhibition of both ON and OFF photoreceptor-bipolar cell synapses with glutamatergic blockers (APB and PDA).

Ribbon synapses exist between bipolar cells and both their inward (photoreceptor) and outward (retinal ganglion cell/amacrine cell) synaptic connections. Under scotopic conditions, the retinal ganglion cell contribution to the flash ERG is reported to be minimal except at very low light simulations.<sup>22,33</sup> However, other studies have reported that retinal ganglion cells, along with bipolar cells, can contribute to OP generation.<sup>53,57</sup> In addition, OPs are also influenced by inhibitory feedback circuits, such as those regulated by amacrine cells.<sup>52,56</sup> Therefore to reduce the influence of retinal ganglion cell and amacrine cell-generated OPs, we injected TTX, which, as a voltage-gated Na<sup>+</sup> channel blocker, prevents spiking of retinal neurons that employ these channels. Interestingly, although APB/PDA treatment completely abolished OP differences between wild-types and RIBEYE knock-outs, treatment with TTX did not reduce the increased OP/b-wave amplitude ratio seen in the RIBEYE knock-out. Therefore, the differences in OPs arise from retinal synaptic activity, which is blocked by APB/PDA but is independent from augmentation of the signals by voltage-dependent Na<sup>+</sup> channels and action potential impulse propagation, as demonstrated by blockade with TTX.

Oscillations in the inner retina are also induced in some retinal disease models, such as the rd1 mouse, in which photoreceptor cells become dysfunctional, although at lower frequencies than the increased OPs in the RIBEYE knock-out.<sup>30,58</sup> Similarly, one model of retinitis pigmentosa involving a rhodopsin mutation that gives rise to photoreceptor degeneration was observed to result in exaggerated OPs during the period before photoreceptor function was impaired.<sup>39</sup> The authors suggest that a disturbance in the retinal circuitry may give rise to an imbalance in signals, resulting in increased OPs. Alternatively, the altered OPs may arise from a disturbance in amacrine cell activity, which has been proposed to be involved in their generation.<sup>52,56,58</sup> Under scotopic conditions, rod photoreceptors communicate classically via rod ON bipolar cells to AII amacrine cells, from where they activate ganglion cells via cone bipolar cells, although alternative pathways have also been described.<sup>59</sup> Interestingly, the hyper-oscillatory potentials observed in models of retinitis pigmentosa have been suggested to arise potentially from an impaired negative feedback loop between bipolar cells and amacrine cells, which in turn may result from impaired photoreceptor inputs, giving rise to increased oscillatory spike activity in ganglion cells.<sup>60</sup> In the RIBEYE knock-out, this feedback loop might be disturbed either at the level of the photoreceptor inputs to the bipolar cell or at the outputs to the amacrine cell (which were shown to have a reduction in fast and sustained transmission by path-clamp recordings<sup>13</sup>). Thus, the role of feedback loops might amplify subtle synaptic defects occurring at the cellular level such that they are detectable at the global ERG level. Of interest, complexins 3/4 (Cpx3/4), which bind retinal SNARE complexes, are located at ribbon synapses.<sup>61</sup> Deletion of Cpx3/4 also leads to reduced b-waves in the ERG however with decreased

OPs.<sup>61</sup> Therefore, the increased OPs appear to be related to ribbon-specific signaling.

In conclusion, deletion of the synaptic ribbon component RIBEYE, which leads to a loss of synaptic ribbons, results in an alteration in the retinal light response as assessed by ERG. The precise contribution of RIBEYE and synaptic ribbons to synaptic transmission is currently being elucidated, but this study demonstrates that its absence leads to a disturbance at the global retinal level, which is particularly manifest in the generation of OPs. Because ribbon synapses occur between multiple cell types of the retina and are involved in both ON and OFF pathways, as well as in circuitry involving both rods and cones, future studies are needed to determine their varying contributions to the connectivity of different neuronal subtypes.

### Acknowledgments

The authors thank Gabriele Kiefe, Sabine Schmidt, and Katharina Wolpert for excellent technical assistance.

Supported by grants from the German Research Foundation/DFG (FOR 2289 and Schm 797/8-1) and by a research grant from the Dr. Rolf M. Schwiete Foundation. We acknowledge support from the Interdisciplinary Neurobehavioral Core at Heidelberg University.

Disclosure: **R. Fairless**, None; **S.K. Williams**, None; **R. Katiyar**, None; **S. Maxeiner**, None; **F. Schmitz**, None; **R. Diem**, None

### References

- Sterling P, Matthews G. Structure and function of ribbon synapses. *Trends Neurosci.* 2005;28:20–29.
- Matthews G, Fuchs P. The diverse roles of ribbon synapses in sensory neurotransmission. *Nat Rev Neurosci.* 2010;11:812–822.
- Zenisek D, Steyer JA, Almers W. Transport, capture and exocytosis of single synaptic vesicles at active zones. *Nature.* 2000;406:849–854.
- Singer JH, LassoVA, Vardi N, Diamond JS. Coordinated multivesicular release at a mammalian ribbon synapse. *Nat Neurosci.* 2004;7:826–833.
- Jackman SL, Choi SY, Thoreson WB, Rabl K, Bartoletti TM, Kramer RH. Role of the synaptic ribbon in transmitting the cone light response. *Nat Neurosci.* 2009;12:303–310.
- Lee BB, Martin PR, Grunert U. Retinal connectivity and primate vision. *Prog Retin Eye Res.* 2010;29:622–639.
- Hoon M, Okawa H, Della Santina L, Wong RO. Functional architecture of the retina: development and disease. *Prog Retin Eye Res.* 2014;42:44–84.
- Helmstaedter M, Briggman KL, Turaga SC, Jain V, Seung HS, Denk W. Connectomic reconstruction of the inner plexiform layer in the mouse retina. *Nature.* 2013;500:168–174.
- Behrens C, Schubert T, Haverkamp S, Euler T, Berens P. Connectivity map of bipolar cells and photoreceptors in the mouse retina. *Elife.* 2016;5:e20041.
- Rogerson LE, Behrens C, Euler T, Berens P, Schubert T. Connectomics of synaptic microcircuits: lessons from the outer retina. *J Physiol.* 2017;595:5517–5524.
- Thoreson WB, Dacey DM. Diverse cell types, circuits, and mechanisms for color vision in the vertebrate retina. *Physiol Rev.* 2019;99:1527–1573.
- Schmitz F, Konigstorfer A, Sudhof TC. RIBEYE, a component of synaptic ribbons: a protein's journey through evolution provides insight into synaptic ribbon function. *Neuron.* 2000;28:857–872.
- Maxeiner S, Luo F, Tan A, Schmitz F, Sudhof TC. How to make a synaptic ribbon: RIBEYE deletion abolishes ribbons in retinal synapses and disrupts neurotransmitter release. *EMBO J.* 2016;35:1098–1114.
- Stojic A, Fairless R, Beck SC, et al. Murine autoimmune optic neuritis is not phenotypically altered by the retinal degeneration 8 mutation. *Invest Ophthalmol Vis Sci.* 2017;58:318–328.
- Sothilingam V, Muhlfriedel R, Tanimoto N, Seeliger MW. In-depth functional analysis of rodents by full-field electroretinography. *Methods Mol Biol.* 2018;1715:207–213.
- Moser T, Grabner CP, Schmitz F. Sensory processing at ribbon synapses in the retina and the cochlea. *Physiol Rev.* 2020;100:103–144.
- Applebury ML, Antoch MP, Baxter LC, et al. The murine cone photoreceptor: a single cone type expresses both S and M opsins with retinal spatial patterning. *Neuron.* 2000;27:513–523.
- Wang YV, Weick M, Demb JB. Spectral and temporal sensitivity of cone-mediated responses in mouse retinal ganglion cells. *J Neurosci.* 2011;31:7670–7681.
- Rao-Mirotnik R, Harkins AB, Buchsbaum G, Sterling P. Mammalian rod terminal: architecture of a binary synapse. *Neuron.* 1995;14:561–569.
- Haverkamp S, Grunert U, Wässle H. The cone pedicle, a complex synapse in the retina. *Neuron.* 2000;27:85–95.
- Regus-Leidig H, Brandstatter JH. Structure and function of a complex sensory synapse. *Acta Physiol (Oxf).* 2012;204:479–486.
- Bui BV, Fortune B. Ganglion cell contributions to the rat full-field electroretinogram. *J Physiol.* 2004;555:153–173.
- Saszik SM, Robson JG, Frishman LJ. The scotopic threshold response of the dark-adapted electroretinogram of the mouse. *J Physiol.* 2002;543:899–916.
- Shirato S, Maeda H, Miura G, Frishman LJ. Postreceptoral contributions to the light-adapted ERG of mice lacking b-waves. *Exp Eye Res.* 2008;86:914–928.
- Dong CJ, Agey P, Hare WA. Origins of the electroretinogram oscillatory potentials in the rabbit retina. *Vis Neurosci.* 2004;21:533–543.
- Cui J, Pan ZH. Two types of cone bipolar cells express voltage-gated Na<sup>+</sup> channels in the rat retina. *Vis Neurosci.* 2008;25:635–645.
- Tian M, Jarsky T, Murphy GJ, Rieke F, Singer JH. Voltage-gated Na channels in AII amacrine cells accelerate scotopic light responses mediated by the rod bipolar cell pathway. *J Neurosci.* 2010;30:4650–4659.
- Wu C, Ivanova E, Cui J, Lu Q, Pan ZH. Action potential generation at an axon initial segment-like process in the axonless retinal AII amacrine cell. *J Neurosci.* 2011;31:14654–14659.
- Trenholm S, Borowska J, Zhang J, et al. Intrinsic oscillatory activity arising within the electrically coupled AII amacrine-ON cone bipolar cell network is driven by voltage-gated Na<sup>+</sup> channels. *J Physiol.* 2012;590:2501–2517.
- Choi H, Zhang L, Cembrowski MS, et al. Intrinsic bursting of AII amacrine cells underlies oscillations in the rd1 mouse retina. *J Neurophysiol.* 2014;112:1491–1504.
- Reifler AN, Chervenak AP, Dolikian ME, et al. All spiking, sustained ON displaced amacrine cells receive gap-junction input from melanopsin ganglion cells. *Curr Biol.* 2015;25:2763–2773.
- Sakai T, Kondo M, Ueno S, Koyasu T, Komeima K, Terasaki H. Supernormal ERG oscillatory potentials in transgenic rabbit with rhodopsin P347L mutation and retinal degeneration. *Invest Ophthalmol Vis Sci.* 2009;50:4402–4409.
- Smith BJ, Wang X, Chauhan BC, Cote PD, Tremblay F. Contribution of retinal ganglion cells to the mouse electroretinogram. *Doc Ophthalmol.* 2014;128:155–168.

34. Becker S, Jayaram H, Holder GE, Limb GA. Short communication: contribution of voltage-gated sodium channels to the rabbit cone electroretinograms. *Curr Eye Res.* 2016;41:569–573.
35. Schmitz F. The making of synaptic ribbons: how they are built and what they do. *Neuroscientist.* 2009;15:611–624.
36. Okawa H, Yu WQ, Matti U, et al. Dynamic assembly of ribbon synapses and circuit maintenance in a vertebrate sensory system. *Nat Commun.* 2019;10:2167.
37. Shen Y, Heimel JA, Kamermans M, Peachey NS, Gregg RG, Nawy S. A transient receptor potential-like channel mediates synaptic transmission in rod bipolar cells. *J Neurosci.* 2009;29:6088–6093.
38. Pattnaik BR, Shahi PK, Marino MJ, et al. A novel KCNJ13 nonsense mutation and loss of Kir7.1 channel function causes Leber congenital amaurosis (LCA16). *Hum Mutat.* 2015;36:720–727.
39. Banin E, Cideciyan AV, Aleman TS, et al. Retinal rod photoreceptor-specific gene mutation perturbs cone pathway development. *Neuron.* 1999;23:549–557.
40. Zencak D, Schouwey K, Chen D, et al. Retinal degeneration depends on Bmi1 function and reactivation of cell cycle proteins. *Proc Natl Acad Sci U S A.* 2013;110:E593–E601.
41. Nishiguchi KM, Carvalho LS, Rizzi M, et al. Gene therapy restores vision in rd1 mice after removal of a confounding mutation in Gpr179. *Nat Commun.* 2015;6:6006.
42. Kolandaivelu S, Chang B, Ramamurthy V. Rod phosphodiesterase-6 (PDE6) catalytic subunits restore cone function in a mouse model lacking cone PDE6 catalytic subunit. *J Biol Chem.* 2011;286:33252–33259.
43. Sato S, Omori Y, Katoh K, et al. Pikachurin, a dystroglycan ligand, is essential for photoreceptor ribbon synapse formation. *Nat Neurosci.* 2008;11:923–931.
44. Nagaya M, Ueno S, Kominami T, et al. Pikachurin protein required for increase of cone electroretinogram b-wave during light adaptation. *PLoS One.* 2015;10:e0128921.
45. Dick O, tom Dieck S, Altmann WD, et al. The presynaptic active zone protein bassoon is essential for photoreceptor ribbon synapse formation in the retina. *Neuron.* 2003;37:775–786.
46. Lindstrom SH, Ryan DG, Shi J, DeVries SH. Kainate receptor subunit diversity underlying response diversity in retinal OFF bipolar cells. *J Physiol.* 2014;592:1457–1477.
47. Puthussery T, Percival KA, Venkataramani S, Gayet-Primo J, Grunert U, Taylor WR. Kainate receptors mediate synaptic input to transient and sustained OFF visual pathways in primate retina. *J Neurosci.* 2014;34:7611–7621.
48. Tsukamoto Y, Omi N. OFF bipolar cells in macaque retina: type-specific connectivity in the outer and inner synaptic layers. *Front Neuroanat.* 2015;9:122.
49. Beaudoin DL, Kupershtok M, Demb JB. Selective synaptic connections in the retinal pathway for night vision. *J Comp Neurol.* 2019;527:117–132.
50. Jean P, Lopez de la Morena D, Michanski S, et al. The synaptic ribbon is critical for sound encoding at high rates and with temporal precision. *Elife.* 2018;7:e29275.
51. Becker L, Schnee ME, Niwa M, et al. The presynaptic ribbon maintains vesicle populations at the hair cell afferent fiber synapse. *Elife.* 2018;7:e30241.
52. Wachtmeister L, Dowling JE. The oscillatory potentials of the mudpuppy retina. *Invest Ophthalmol Vis Sci.* 1978;17:1176–1188.
53. Wachtmeister L. Oscillatory potentials in the retina: what do they reveal. *Prog Retin Eye Res.* 1998;17:485–521.
54. Hare WA, Ton H. Effects of APB, PDA, and TTX on ERG responses recorded using both multifocal and conventional methods in monkey. Effects of APB, PDA, and TTX on monkey ERG responses. *Doc Ophthalmol.* 2002;105:189–222.
55. Lei B, Yao G, Zhang K, Hofeldt KJ, Chang B. Study of rod- and cone-driven oscillatory potentials in mice. *Invest Ophthalmol Vis Sci.* 2006;47:2732–2738.
56. Dai J, He J, Wang G, Wang M, Li S, Yin ZQ. Contribution of GABA<sub>A</sub>, GABA<sub>C</sub> and glycine receptors to rat dark-adapted oscillatory potentials in the time and frequency domain. *Oncotarget.* 2017;8:77696–77709.
57. Gauvin M, Dorfman AL, Trang N, et al. Assessing the contribution of the oscillatory potentials to the genesis of the photopic ERG with the discrete wavelet transform. *Biomed Res Int.* 2016;2016:2790194.
58. Borowska J, Trenholm S, Awatramani GB. An intrinsic neural oscillator in the degenerating mouse retina. *J Neurosci.* 2011;31:5000–5012.
59. Soucy E, Wang Y, Nirenberg S, Nathans J, Meister M. A novel signaling pathway from rod photoreceptors to ganglion cells in mammalian retina. *Neuron.* 1998;21:481–493.
60. Margolis DJ, Detwiler PB. Cellular origin of spontaneous ganglion cell spike activity in animal models of retinitis pigmentosa. *J Ophthalmol.* 2011;2011:507037.
61. Reim K, Regus-Leidig H, Ammermuller J, et al. Aberrant function and structure of retinal ribbon synapses in the absence of complexin 3 and complexin 4. *J Cell Sci.* 2009;122:1352–1361.